KeAi

CHINESE ROOTS
GLOBAL IMPACT

#### Contents lists available at ScienceDirect

### Petroleum Science

journal homepage: www.keaipublishing.com/en/journals/petroleum-science



### **Original Paper**

## Probing the influence of secondary fracture connectivity on fracturing fluid flowback efficiency



Yi-Ning Wu <sup>a</sup>, Li-Sha Tang <sup>a</sup>, Yuan Li <sup>a</sup>, Li-Yuan Zhang <sup>a, \*\*</sup>, Xu Jin <sup>b, \*</sup>, Ming-Wei Zhao <sup>a</sup>, Xiang Feng <sup>c</sup>, Cai-Li Dai <sup>a</sup>

- <sup>a</sup> School of Petroleum Engineering, China University of Petroleum (East China), Qingdao, 266580, Shandong, China
- <sup>b</sup> Research Institute of Petroleum Exploration & Development, PetroChina, Beijing 100083, China
- <sup>c</sup> College of Chemistry and Chemical Engineering, China University of Petroleum (East China), Qingdao, 266580, Shandong, China

#### ARTICLE INFO

# Article history: Received 27 June 2022 Received in revised form 13 October 2022 Accepted 18 October 2022 Available online 21 October 2022

Edited by Yan-Hua Sun

Keywords:
Fracturing fluid
Secondary fracture connectivity
Flowback efficiency
Dual media
Microfluidic model

#### ABSTRACT

A deep understanding of the geometric impacts of fracture on fracturing fluid flowback efficiency is essential for unconventional oil development. Using nuclear magnetic resonance and 2.5-dimensional matrix-fracture visualization microfluidic models, qualitative and quantitative descriptions of the influences of connectivity between primary fracture and secondary fracture on flowback were given from core scale to pore network scale. The flow patterns of oil-gel breaking fluid two-phase flow during flowback under different fracture connectivity were analyzed. We found some counterintuitive results that non-connected secondary fracture (NCSF, not connect with artificial primary fracture and embedded in the matrix) is detrimental to flowbackefficiency. The NCSF accelerates the formation of oil channeling during flowback, resulting in a large amount of fracturing fluid trapped in the matrix, which is not beneficial for flowback. Whereas the connected secondary fracture (CSF, connected with the artificial primary fracture) is conducive to flowback. The walls of CSF become part of primary fracture, which expands the drainage area with low resistance, and delays the formation of the oil flow channel. Thus, CSF increases the high-speed flowback stage duration, thereby enhancing the flowback efficiency. The fracturing fluid flowback efficiency investigated here follows the sequence of the connected secondary fracture model (72%) > the matrix model (66%) > the non-connected secondary fracture model (38%). Our results contribute to hydraulic fracturing design and the prediction of flowback efficiency.

© 2023 The Authors. Publishing services by Elsevier B.V. on behalf of KeAi Communications Co. Ltd. This is an open access article under the CC BY-NC-ND license (http://creativecommons.org/licenses/by-nc-nd/4.0/).

### 1. Introduction

Low permeability oil and gas resources, such as tight oil and shale oil and gas, are essential to ensure world energy security (Du et al., 2014; Jia et al., 2021; Lu et al., 2018; Wang et al., 2016; Zou et al., 2010, 2013). However, increasing the production rate by simply injecting chemicals is challenging due to low permeability. Thus, creating an effective complicated fracture network and enhancing the imbibition effect of fracturing fluid are crucial for increasing the yield. To enhance oil recovery, hydraulic fracturing technology is an effective way to generate high-speed seepage

E-mail addresses: 20210085@upc.edu.cn (L.-Y. Zhang), jinxu@petrochina.com.cn (X. lin).

channels (Wu et al., 2012; Zou et al., 2015; Pak and Chan, 2004).

As the 'blood' of the hydraulic fracturing processes, the performance of fracturing fluid is one of the main factors affecting oil and gas production after fracturing. Guar gum, a mainstream polymer fracturing fluid, possesses a good thickening ability that multiple crosslinking agents can crosslink to form a fracturing gel. However, the concentration of guar gum is relatively high and contains insoluble proteins, resulting in a high risk of reservoir contamination after fracturing gel breaking (Garcia and Andrade, 1997; Grasdalen and Painter, 1980; Mccleary et al., 1985). To decrease the contamination, clean fracturing fluid composed of surfactants can selfassemble into wormlike micelles and form a three-dimensional network structure to carry proppants (Howe et al., 2015). Micelles in the fracturing fluid will automatically break after contact with oil, leaving a negligible amount of solid residual and damage to the reservoir. Nevertheless, the low viscosity of clean fracturing fluid after gel breaking makes it more susceptible to geometric features of

<sup>\*</sup> Corresponding author.

<sup>\*\*</sup> Corresponding author.

dual media than traditional polymer fracturing fluid. Thus, the flowback state and efficiency of gel breaking fluid are influenced not only by the competition between viscous and capillary forces but also by geometric properties such as secondary fracture connectivity (Du et al., 2019a, b; Garcia and Andrade, 1997; Grasdalen and Painter, 1980; Zhu et al., 2021). Due to diagenesis or hydraulic fracturing, secondary fractures form in formation. After hydraulic fracturing, the fracturing fluid penetrating the matrix will activate dormant natural fractures or develop new secondary fractures due to high pressure (Liang et al., 2019). The secondary fractures embedded in the matrix show different geometric characteristics, where some are connected with artificial primary fractures, denoted as CSF. We refer to those not connected as non-connected secondary fractures, NCSF. The secondary fractures and matrix together compose complex dual media. The influence of the secondary fracture connectivity on fracturing fluid unstable flow and flowback efficiency has not been extensively studied. To explore the fracturing mechanism, mathematical modeling or numerical simulation (Wang et al., 2016) can accurately simulate the fracture morphology of a natural reservoir, requiring a large amount of data analysis due to small grid division (Liu et al., 2015; Wang, 2015). Nuclear magnetic resonance (NMR) can characterize the complex 3D core structure and clarify the multiphase flow of fracturing fluid and crude oil (Longoria et al., 2015). Through the analysis of the  $T_2$  spectrum (Cheng et al., 2019; Xu et al., 2020; Zhang et al., 2019, 2020), Zhang et al. found that the larger the surface roughness and bending degree of the secondary fractures, the more fracturing fluid detained in the secondary fractures (Zhang et al., 2019). However, the flow pattern of fluid in cores can not be directly observed by NMR. Microfluidic technology has been widely used to study unstable two-phase flow behavior in porous media (Bowden et al., 2010; Chatzis et al., 1983; Chatzis, 2009; Song and Kovscek, 2015), including low salinity water flooding, chemical flooding, filtration and flowback of fracturing fluids (Abedi et al., 2012; Bartels et al., 2016; He et al., 2017; Howe et al., 2015; Kianinejad et al., 2013; Liang et al., 2019; Mehmani et al., 2017; Morteza, 2019; Nilsson et al., 2013; Sedaghat et al., 2013; Schumi et al., 2019; Sinz et al., 2013; Tangirala and Sheng, 2019). These microfluidic models for studying the flowback characteristic were basically homogeneous pores on a 2D device. The research mainly focuses on the influences of additives in fracturing fluid on flowback efficiency. Although it was found that the existence of fractures significantly affected the unstable two-phase flow, few detailed studies investigating the influence of geometric properties, such as fracture type and connectivity on flowback could be found. Moreover, the traditional two-dimensional microfluidic models only vary the discrepancy between pore and throat, limiting their ability to mimic the nature reservoir. As such, some representative multiphase flow phenomena are hard to be observed in the twodimensional models, such as the pinch-off when bubbles or oil droplets pass through the pore throat units (Xu et al., 2017). Moreover, the flowback process of fracturing fluid also involves oil-water two-phase flow. Thus, the traditional 2D model cannot reflect the flowback characteristics of gel-breaking fluid. The material commonly used for making microfluidic models (polydimethylsiloxane) has oil-wet property and permeability, but it is hard to fabricate 3D models. 2.5D visualized models were selected for the experiments to obtain the flow pattern in core. Xu et al. proposed a 2.5-dimensional model to simulate the real formation situation (Xu et al., 2017). The throat size is differed from the pore in the horizontal direction and in-depth. The 2.5-D model has been successfully applied to study low salinity water flooding (Du et al., 2019a, b) and nano-particle flooding (Agrawal et al., 2018).

Here, we combined a 2.5-D fracture-matrix model and nuclear magnetic resonance to investigate the influence of secondary fracture connectivity on oil-water two-phase flow. We aimed to gain more insights into the flowback mechanism of fracturing fluid in dual media.

### 2. Materials and methods

#### 2.1. Materials and instruments

Oleamide propyl dimethylamine PKO was supplied by Shanghai Chuxing Chemical Co., Ltd. Sodium *p*-toluenesulfonate CHO and kerosene were purchased from Shanghai Aladdin Biochemical Technology Co., Ltd. Mineral oil was purchased from Shanghai Macklin Biochemical Technology Co., Ltd. Sudan red oil-soluble dye and bright blue water-soluble dyes were supplied by Tianjin Guangxia Fine Chemical Research Institute.

The instruments used include nuclear magnetic resonance analysis and imaging system (Suzhou Niumag Analytical Instruments Co., Ltd), TC150 six-speed viscometer (BROOKFIELD, U.S.A.), high precision injector (Hamilton, U.S.A.) and micro-flow pump (Harvard, U.S.A.).

### 2.2. Microchannel structure design

To effectively reflect the influences of geometric properties on the flowback process, three micro-models were fabricated according to the different fracture properties. The microstructure is shown in Fig. 1. The three microfluidic models are denoted as S1, S2 and S3, respectively, where ① represents the matrix, ② represents connected secondary fracture (CSF), ③ represents non-connected secondary fracture (NCSF), ④ represents the stable boundary at in-depth formation, and ⑤ represents the primary fracture. S1 is a matrix model with only pore throat units. S2 is a connected secondary fracture model and S3 is a non-connected secondary fracture model. The fracture with a length of 2.5 cm and a depth of 20  $\mu$ m locates at the center of the matrix. The widths of the three-section fracture are 1500, 1000, and 500  $\mu$ m, respectively, to simulate the gradual nip-out morphology.

The three microfluidic models have the same injection end (distal boundary) and exit end (primary fracture). The diversion design of the injection end is mainly to obtain a uniform flow and a more stable injection rate. The size of the pore throat model is as follows: the pore width is 150  $\mu m$ , the depth is 20  $\mu m$ , the throat is 20  $\mu m$  wide and 3  $\mu m$  deep and the total matrix size is 3.0 cm  $\times$  1.5 cm.

### 2.3. Core drainage experiments

The dimensionless length of fractures reflects the degree of nipout of fractures in the formation. The cores were cut along the flow direction and cemented in one end as shown in Fig. 2. The bonded

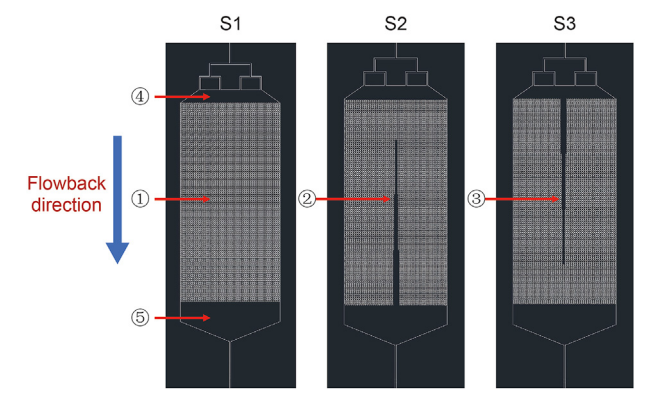


Fig. 1. 2.5D schematic diagram of a microstructure model.

length to fracture length ratio is denoted as the dimensionless length of fractures. The secondary fractured core model is shown in Fig. 2 (the dimensionless length of fractures is 70%).

NMR experiments of flowback efficiency were carried out with systems including matrix core, connected secondary fracture core and non-connected secondary fracture core. The physical parameters of the cores are shown in Table 1. The production pressure difference was 1.022 MPa, the confining pressure was 10 MPa, the soaking time was 24 h, and the test time was 330 min. The viscosity of simulated oil was of 2.4 mPa s. The gel breaker used without NMR signal was prepared with heavy water and the viscosity was maintained at 1.1 mPa s. The device used in the core experiment and its connection diagram is shown in Fig. S1 in Supporting Information. The detailed experimental procedures of core physical simulation and microfluidic experiments are presented in Supporting Information.

### 2.4. Computing methods

The calculation formula of fracturing fluid flowback efficiency in Fig. 3 is as follows:

$$\eta = \frac{Q_1 + Q_2}{O} \tag{1}$$

where  $\eta$  is the flowback efficiency, %;  $Q_1$  is the flowback volume before fracture closure, mL;  $Q_2$  is the flowback volume after fracture closure, mL; Q is the total injection volume, mL.

The dimensionless capillary number *Ca* was used to reflect the ratio of viscous force to capillary force in the flowback process. The expression in the microfluidic model is:

$$Ca = \frac{Q\mu_{\rm W}}{h_{\rm p}w_{\rm p}\sigma\phi} \tag{2}$$

where Q is the injection flow,  $m^3/s$ ;  $\mu_W$  is the viscosity of gel breaking fluid, mPas;  $h_p$  is the pore height, m;  $w_p$  is the pore width, m;  $\sigma$  is the oil-water interfacial tension, mN/m;  $\phi$  is the microfluidic model porosity, 61.62%.

### 3. Results and discussion

3.1. The influences of secondary fracture connectivity on fracturing fluid flowback in cores

### 3.1.1. Flowback efficiency in cores under different fracture connectivity

According to previous research, the fracture network would affect the flowback efficiency (Tompkins et al., 2016; Gao et al., 2013; Zhang et al., 2011). This paper is primarily concerned with

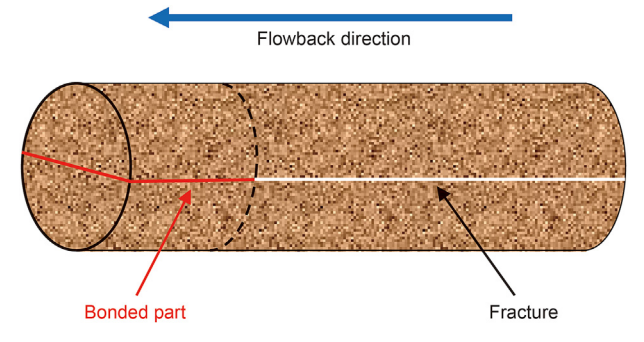


Fig. 2. Non-connected secondary fracture core model.

the influences of secondary fracture connectivity on flowback efficiency in cores as shown in Fig. 3. Flowback efficiency is the ratio of the sum of flowback before and after fracture closure to the injection volume. Under the same experimental conditions, the flowback efficiency of matrix core and connected secondary fracture core were higher, which were 65.49% and 72.46%, respectively. While the flowback efficiency in non-connected secondary fracture core was only 37.75%. Moreover, the initial flowback rate of the CSF core and the matrix core was higher as shown in Fig. 3, and the high-speed flowback stage was longer than in NCSF core according to Fig. 3, thus leading to a higher total flowback efficiency.

### 3.1.2. Flowback characteristics in cores investigated by nuclear magnetic resonance T<sub>2</sub> spectrum

To further clarify the core physical simulation results, the whole flowback process of fracturing fluid was monitored by low field nuclear magnetic resonance. The influences of the secondary fracture connectivity on oil-water two-phase flow characteristics were studied. T<sub>2</sub> spectrums at different times during flowback are shown in Fig. 4. Fig. 4a and b shows the flowback of gel-breaking fluid in the matrix core. The flowback process can be divided into two stages according to T<sub>2</sub> spectrum: oil-water two-phase highspeed (0-45 min) and low-speed (45-300 min) migration. At the beginning of the flowback, the core was mainly saturated with gelbreaking fluid and the overall signal was low. After 5 min, the signal in the large pores increased significantly, indicating that the oil phase started to enter the large pores. The signal in large pores continuously increased when the flowback proceeded to 15-30 min. And the composition of output liquid changed from single gel breaking liquid to the oil-water two-phase mixture to simulated oil. In the first stage of flowback (0-45 min), the gelbreaking fluid in the large pores flowed out and the oil phase rapidly penetrated through the large pores to form an oil channel. This stage was named the high-speed flowback stage. In the initial second flowback stage (45-60 min), the signal in the oil flow channel decreased slightly, indicating that the oil flow channel formed in the first stage developed into the oil-water two-phase migration channel. With the flowback proceeding, the oil signal in small pores gradually increased. This means simulated oil slowly penetrated into some small pores and displaced the gel-breaking liquid. During 240-300 min, no noticeable change was found, indicating that the two-phase flowback process had finally reached the end.

Fig. 4c shows the  $T_2$  spectrum of the flowback in the connected secondary fracture core. Similar to the flowback characteristics of matrix core, the connected secondary fracture core also experienced the high-speed breakthrough stage of the oil phase. Within 0–30 min, the signal intensity in the large pore, namely, the high-speed channel of oil phase, increased from 280 to 600. At 45 min, the signal intensity of large pores began to decrease. From 180 min, the signal of  $T_2$  spectrum remained almost unchanged. However, for non-connected secondary fractures, the flowback process is different. As shown in Fig. 4d, the duration of the first high-speed flowback stage was shortened from 30 min to less than 5 min, compared with the connected secondary fracture (CSF) core. By comparing the area of  $T_2$  spectrum in the high-speed flowback stage, the amount of gel breaking fluid flowback in CSF core was more considerable than that in the NCSF core.

Furthermore, in the non-connected secondary fracture (NCSF) core, no significant change was found in the  $T_2$  curve between 60 and 300 min. That is to say that the gel-breaking fluid did not immigrate obviously after 60 min. Thus, the total amount of gel breaking fluid flowback in NCSF core was significantly reduced, which was consistent with the flowback efficiency trend shown in Fig. 3.

**Table 1** Physical parameters of cores with different secondary fracture morphology.

Core number	Length, mm	Diameter, mm	Porosity, %	Permeability, $\times 10^{-3}$ $\mu m^2$	Production pressure difference, MPa	Confining pressure, MPa	Soaking time, h	Туре
A-1	46.72	25.36	17.16	3.82	1.022	10.072	24	Matrix core
A-2	50.61	23.57	17.35	3.78	1.022	10.157	24	Connected secondary fracture core
A-3	48.56	23.61	17.35	3.78	1.022	10.013	24	Non-connected secondary fracture core

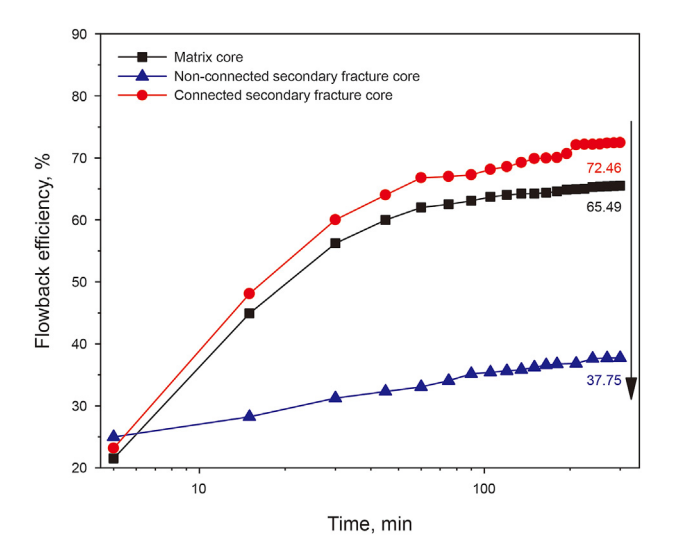


Fig. 3. Flowback efficiency in different cores.

The flowback characteristics were investigated by nuclear magnetic resonance, but how fracture connectivity affects the oilwater two-phase flow in fractures and matrix, respectively, is still unclear.

### 3.2. Two-phase flow in the matrix model

Migration of oil-water flow from matrix to primary fracture during flowback is shown in Fig. 5. Oil supply edge was used to represent in-depth formation and provenance of oil. At the initial time of flowback, the blue gel-breaking fluid filled the matrix as a continuous phase. A small amount of oil phase was sealed in the continuous gel-breaking fluid. In this work, the oil-water two-phase migration during flowback showed the following rules: oil-water two-phase migration did not form an apparent oil-water front at the beginning of flowback.

In contrast, oil phase broke the 'water lock' structure rapidly similar to viscous fingering, forming oil channels from the upstream supply edge to the downstream primary fracture. After 60 s, several oil channels developed, but the flowback efficiency of gel breaking fluid was only 32.45%, providing validation for the NMR results. Then, flowback continued after the formation of the oil channels. The gel-breaking fluid gradually became a discontinuous phase in the matrix and flowed back into the primary fracture in a droplet pattern. After 600 s, the area of blue gel-breaking fluid in the matrix did not change and the ultimate flowback efficiency of the gel-breaking fluid in matrix was about 65.96%.

### 3.3. Two-phase flow in microfluidic models with different secondary fracture connectivity

NMR results indicated that secondary fracture connectivity significantly impacts the flowback efficiency. But it is still difficult

to directly gain insight into the influences of connected/non-connected secondary fractures on the migration mechanism of two-phase flowback by NMR alone. In this section, the flowback of oil and water was directly observed in microfluidic dual media models. The flowback efficiency of fracturing fluid in fracture and matrix was recorded and calculated in real-time to analyze the flowback in dual media.

The roles of connected secondary fracture (CSF) and nonconnected secondary fracture (NCSF) in the flowback process are different. For CSF, the upstream matrix is homogeneous. From 0 to 126 s shown in Fig. 6a, it can be seen that a large proportion of gelbreaking fluids in the upstream matrix was evenly displaced by oil phase. At 213 s, an apparent oil channel was observed. After that, the gel-breaking fluid in the matrix flowed to the primary fracture in the form of discontinuous droplets. The final flowback efficiency was up to 72.23%, higher than that of the matrix model. In contrast, for non-connected secondary fracture model, from 0 to 42 s in Fig. 6b, it can be seen that the oil phase preferentially entered the secondary fracture and the flowback efficiency of the gel breaking fluid in the matrix on both sides of the fracture was low. There was no obvious oil channel in the matrix. The oil phase entered the downstream matrix from the tip of secondary fracture and broke through the water phase into primary fracture at 173 s. In the following time, several small oil channels formed in the downstream matrix and almost no more migration of gel-breaking fluid was observed. The final flowback efficiency was 48.52%, lower than that of the matrix model.

### 3.4. Contribution of secondary fracture during flowback in different models

To verify the proposed flowback mechanism, we calculated the flow of gel-breaking fluid in secondary fracture by image processing. The ratio of volume of gel-breaking fluid flowing through secondary fractures to the total volume of flowback with time was analyzed under the capillary number Ca = 0.05, as shown in Fig. 7.

The gel-breaking fluid in the connected secondary fracture was 11.54% at the starting point, which was less than that (14.18%) in the non-connected secondary fracture. Subsequently, the gel-breaking fluid in the non-connected secondary fracture rapidly decreased to 1.97% within 64 s. At this time, almost all the gel-breaking fluid in the fracture entered the downstream matrix. Then the residual gelbreaking fluid in the fracture remained stable at 1.74%. It is considered that non-connected secondary fractures accelerated the formation of low-resistance oil flow channels and inhibited the occurrence of oil flow channels in the matrix on both sides of fractures, thus, reducing the matrix flowback efficiency.

In contrast, the connected secondary fracture model showed no gel-breaking liquid reduction in the secondary fracture. An increase of 17.97% was found after the beginning of flowback. After that, the gel-breaking liquid in the matrix at the upper end flowed into the fracture, and quickly discharged into the artificial primary fracture through the low resistance secondary fracture, forming an oil flow channel. At 168, 194, 395, 446, and 658 s, the content of gel

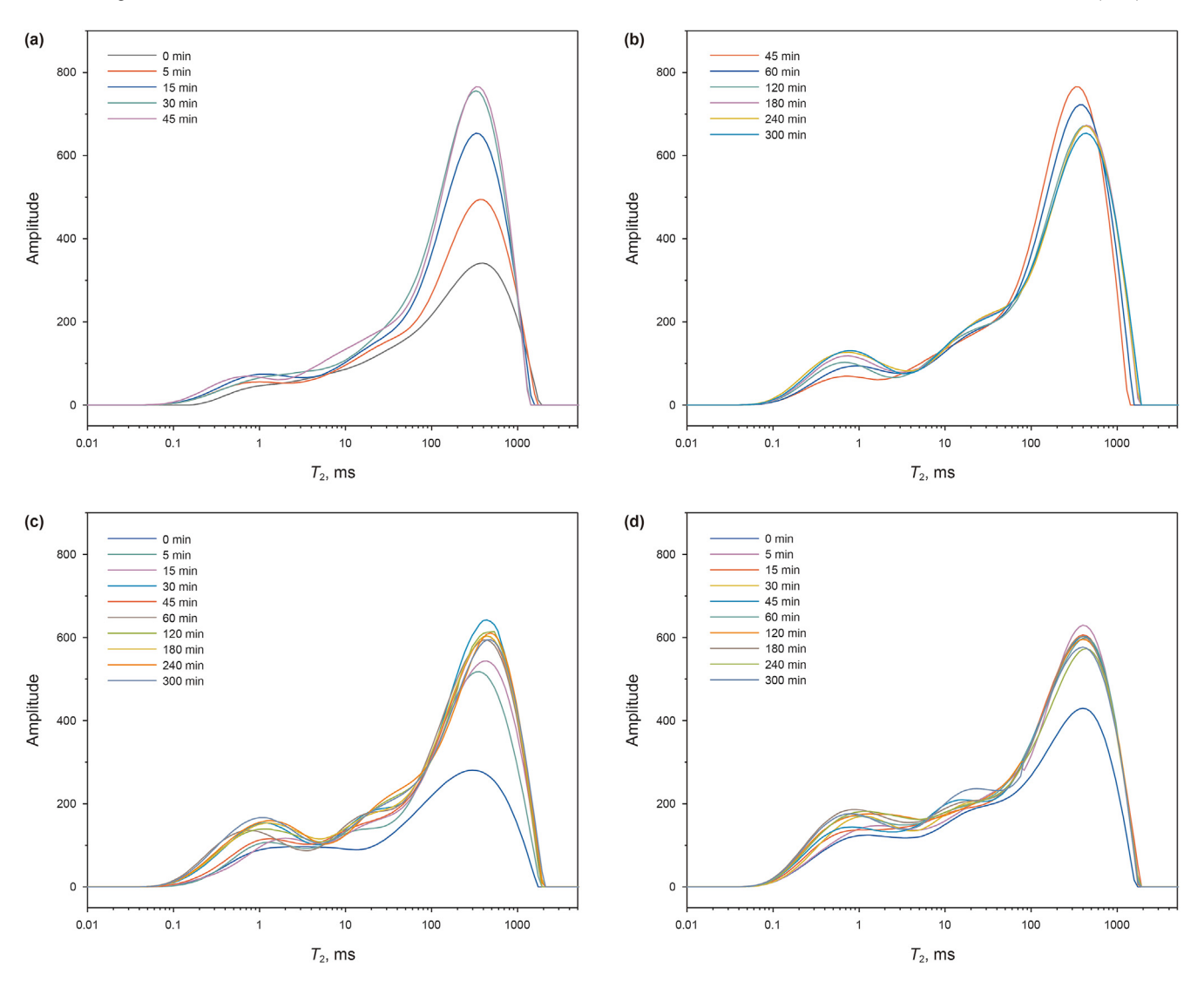
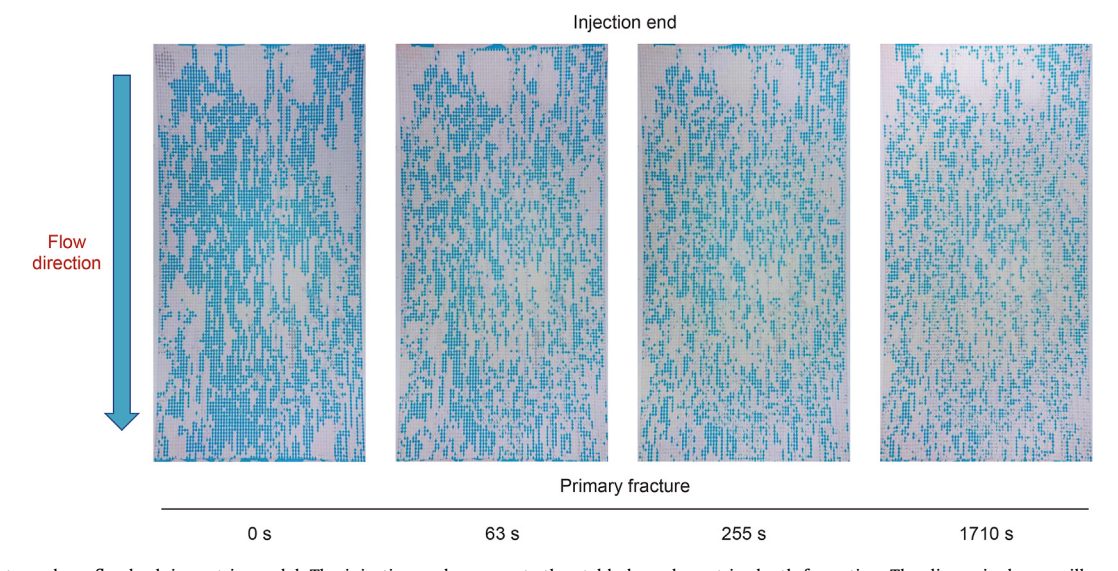
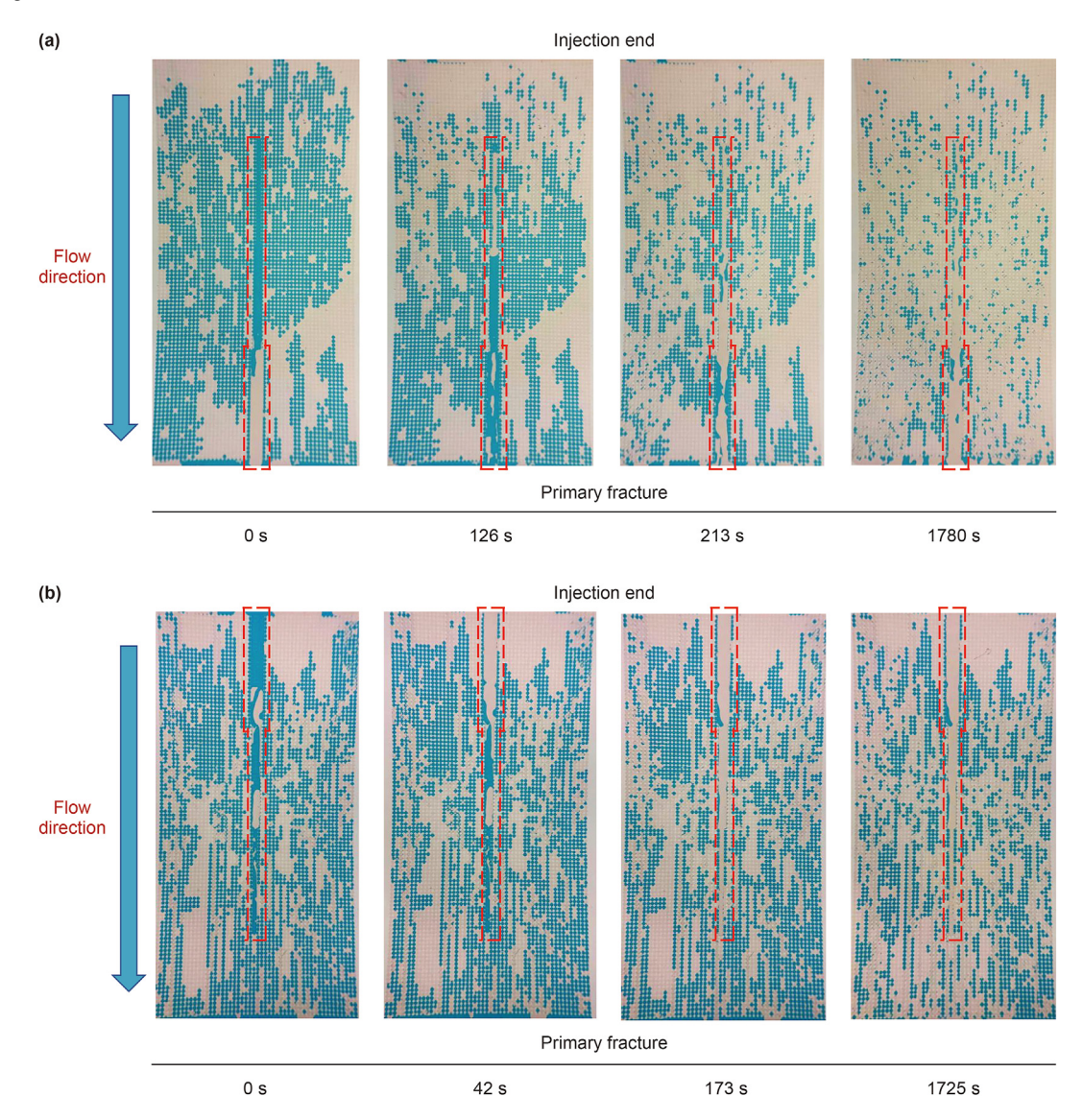


Fig. 4.  $T_2$  spectrums in different flowback times. (**a**, **b**)  $T_2$  spectrum of matrix core; (**c**)  $T_2$  spectrum of connected secondary fracture core; (**d**)  $T_2$  spectrum of non-connected secondary fracture core.



**Fig. 5.** Oil-water two-phase flowback in matrix model. The injection end represents the stable boundary at in-depth formation. The dimensionless capillary number *Ca* corresponding to the actual flowback velocity was set at 0.05.



**Fig. 6.** (a) Oil-water two-phase flowback in connected secondary fracture model with Ca = 0.05; (b) Oil-water two-phase flowback in non-connected secondary fracture model with Ca = 0.05. The injection end represents the stable boundary at in-depth formation.

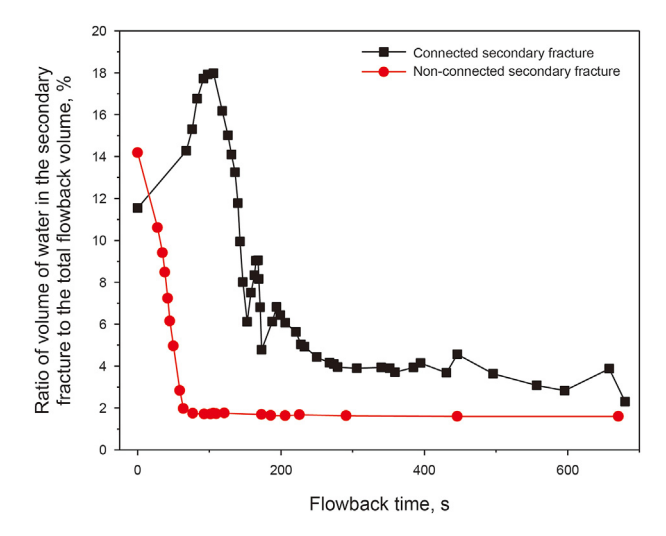


**Fig. 7.** Ratio of the volume of gel breaking fluid flowing in secondary fracture to the total flowback volume with time.

breaking fluid in the secondary fractures increased, indicating that the gel breaking fluid continued to enter the secondary fractures. The connectivity of secondary fractures and main fractures effectively increased the area of drainage zone, maintained the oil phase transport ability in the matrix, and developed low-resistance oil migration channels for gel-breaking fluid.

### 3.5. Contribution of matrix of different geometric properties in connected/non-connected secondary fracture models

To quantitatively analyze the influence of secondary fracture connectivity on the flowback efficiency, the matrix was divided into two categories according to the geometric characteristics: the ones on both sides of secondary fracture (MSF) and the other at the end of secondary fracture (MEF), as shown in Fig. 8. The flowback efficiency of each region was calculated. The results are shown in Fig. 9.

The variation of flowback efficiency of MSF and MEF with time in two models were analyzed at the capillary number Ca = 0.05. It can be seen from Fig. 9a that in the non-connected secondary fracture model, the matrix flowback rate in MSF and MEF increased

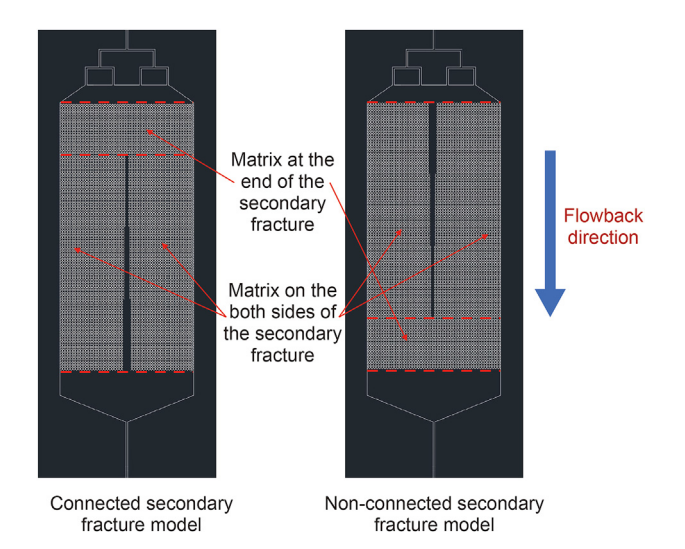


**Fig. 8.** Matrix division according to the geometric characteristics: matrix on both sides of secondary fracture (MSF) and matrix at the end of secondary fracture (MEF).

rapidly at the beginning and reached the maximum in a short time. In the subsequent time, the flowback efficiency did not change significantly. In contrast, in the connected secondary fracture model, the oil phase entered MEF first, and the flowback efficiency in MEF rapidly peaked. However, the flowback rate in MSF showed a different trend. The initial flowback rate quickly increased, then slowed down, but the high-speed flowback stage lasted as long as the 1600s. Therefore, the flowback efficiency was up to 70%.

Based on the above analysis of the two-phase flow in the three models, the flowback characteristics of the fracturing fluid in dual media are summarized in Fig. 10. The secondary fracture and the primary fracture were interlinked for the connected secondary fracture model, this is equivalent to enlarge low-pressure boundary accelerate gel breaking fluid flowing out. Moreover, oil-water two phases flowed from upstream inlet to enlarged outlet, resulting in a flow pattern similar to inverse radial flow. Thus, the resistance of the whole flow is low, leading to a high flowback efficiency of gel breaking fluid in this model. In contrast, in the non-connected secondary fracture model, oil phase entered the fracture-matrix media from the supply edge. It tended to flow into the secondary

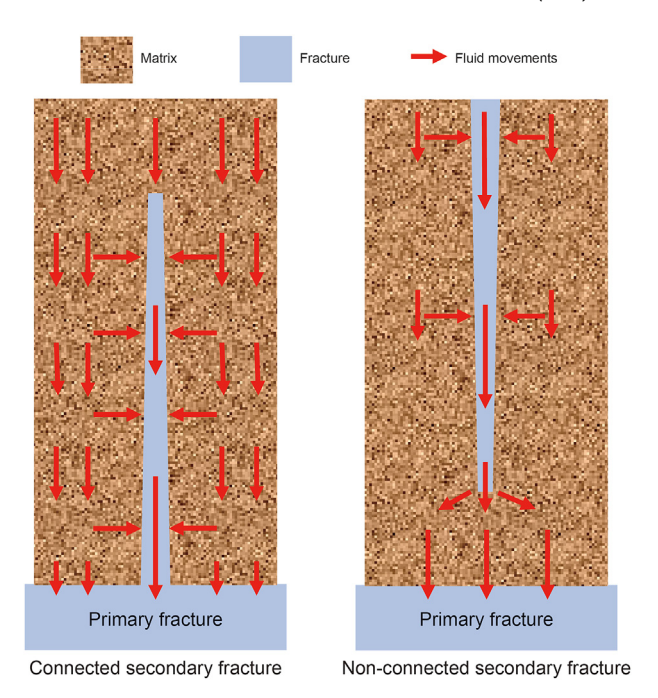


Fig. 10. Schematic diagram of dual media flowback mechanism.

fracture in the first place due to its low flow resistance. Then oil phase entered the matrix from the tip of the secondary fracture. The flowback process was akin to radial flow due to the large inlet and small outlet. The fracturing fluid in the matrix on both sides of the non-connected secondary fracture model is more likely to be trapped in situ, resulting in a much lower final flowback efficiency than the connected secondary fracture model.

### 3.6. Influence of capillary number on flowback efficiency

Oil-water two-phase migration needs to overcome the flow resistance of viscous loss, capillary force and Jamin effect simultaneously. These factors affect the capillary number, which changes the fingering pattern, thus influencing the flowback of fracturing fluid. To simulate the production pressure difference in oilfield, we chose different injection rates, which were in the range of the

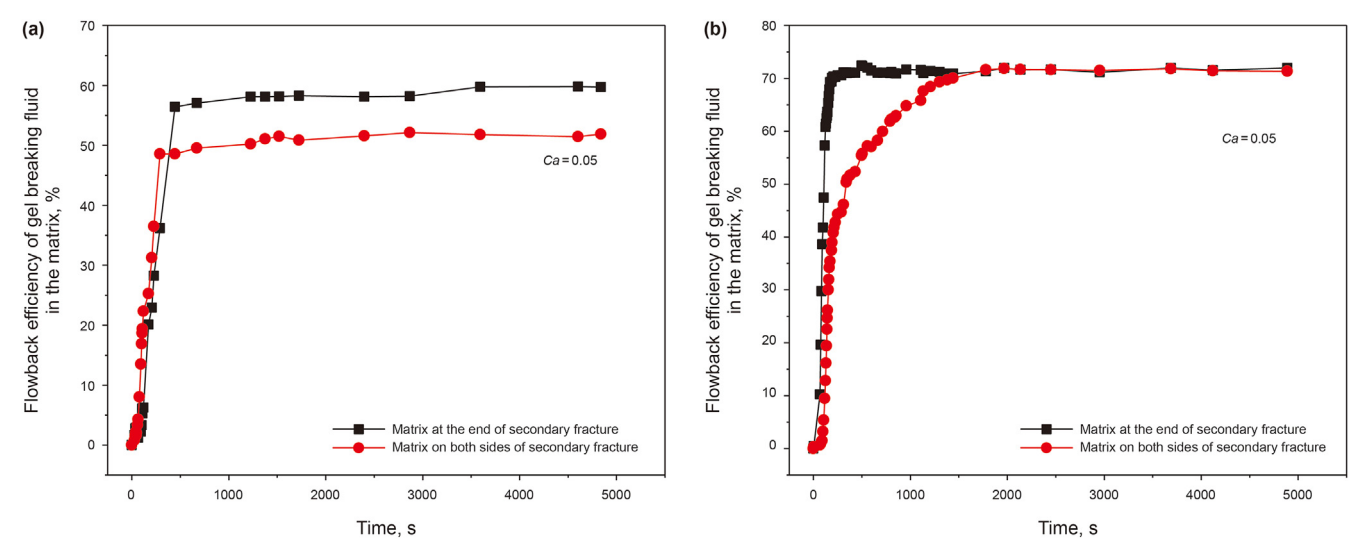


Fig. 9. Flowback efficiency of MSF and MEF in non-connected model (a) and connected secondary fracture model (b).



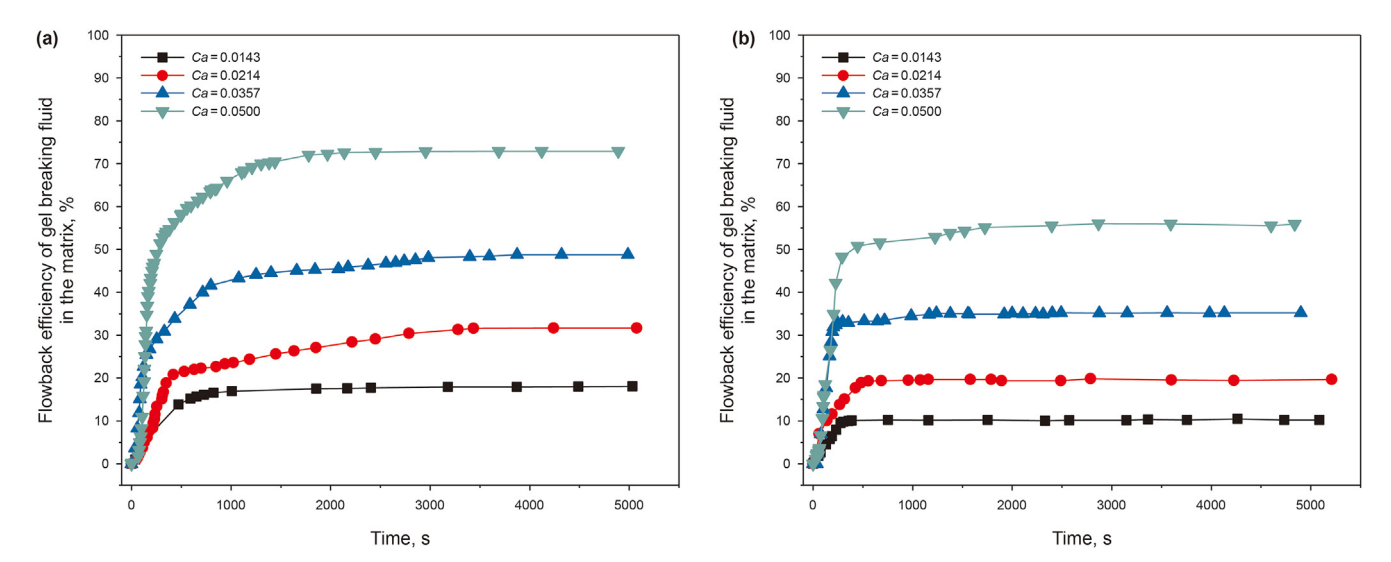


Fig. 11. Flowback efficiency in connected secondary fracture model (a) and non-connected secondary fracture model (b) under different capillary numbers (Ca).

actual flow rate of flowback. Hence, the capillary numbers used in the experiments were 0.0143, 0.0214, 0.0357, and 0.05, respectively. The experiments are all in the viscous fingering scope based on the relationship between capillary numbers (Ca) and water-oil viscosity ratio (*M*) determined the fingering mode of oil-water two-phase migration (Zhang et al., 2011). Moreover, the viscous force mainly affected the oil-water two-phase migration in the flowback process. With the increase in capillary number, the ultimate flowback efficiencies were 18.06%, 31.65%, 49.16%, and 72.89% for connected secondary fracture model, and 10.23%, 19.66%, 35.25%, and 55.89% for non-connected secondary fracture model, respectively, as shown in Fig. 11. Thus, it can be seen that the flowback efficiency increased with Ca. Moreover, the flowback efficiency in the connected secondary fracture model and was always more significant than that in the non-connected secondary fracture model within the Ca scope of the experiments. The details of flowback characteristics in matrix under different Ca are shown in Supporting Information.

### 4. Conclusions

This paper studied the influence of secondary fracture connectivity on the flowback of clean fracturing gel-breaking fluid from the core and micro-pore scales. The two-phase flow characteristics were analyzed in fractures and matrix, respectively. Finally, the flowback mechanism of clean fracturing fluid in dual media was clarified and the following conclusions were obtained:

From the simulation experiments in the core, the connected secondary fracture contributed to the flowback of fracturing fluid, however, the non-connected secondary fracture went against flowback efficiency lower than that in the matrix model. When the secondary fracture was connected with the primary fracture, it provided a high-speed channel for oil-water flowback, expanded the low-pressure drainage zone area, and improved the flowback of gel-breaking fluid located at in-depth formation. Hence, the gelbreaking fluid flowback efficiency was higher than that of the non-connected secondary fracture model.

The above results imply that secondary fracture connectivity also plays a key role during fracturing fluid flowback, like viscosity ratio and wettability of formation. To regulate the flowback efficiency and further enhance oil recovery, the technologic parameters of fracturing need to be adjusted to control the properties of secondary fracture.

### **Declaration of competing interest**

The authors declare that they have no known competing financial interests or personal relationships that could have appeared to influence the work reported in this paper.

### Acknowledgments

This work was supported by the National Key Research and Development Program of China (Grant No. 2019YFA0708700).

### Appendix A. Supplementary data

Supplementary data to this article can be found online at https://doi.org/10.1016/j.petsci.2022.10.014.

### References

Abedi, B., Ghazanfari, M.H., Kharrat, R., 2012. Experimental study of polymer flooding in fractured systems using five-spot glass micromodel: the role of fracture geometrical properties. Energy Explor. Exploit. 30 (5), 689–706. https://doi.org/10.1260/0144-5987.30.5.689.

Agrawal, D., Xu, K., Darugar, Q., Khabashesku, V.N., 2018. Enhanced oil recovery by nanoparticle-induced crude oil swelling: pore-scale experiments and understanding. SPE Asia Pac. Oil Gas Conf. Exhib. https://doi.org/10.2118/191971-MS.

Bartels, W.B., Mahani, H., Berg, S., van der Hoeven, J., Fadili, A., 2016. Low salinity flooding (L.S.F.) in sandstones at pore scale: micro-model development and investigation. SPE Ann. Tech. Conf. Exhib. https://doi.org/10.2118/181386-MS.

Bowden, S.A., Cooper, J.M., Greub, F., Tambo, D., Hurst, A., 2010. Benchmarking methods of enhanced heavy oil recovery using a microscaled bead-pack. Lab Chip 10. https://doi.org/10.1039/B926815D.

Chatzis, I., Morrow, N.R., Lim, H.T., 1983. Magnitude and detailed structure of residual oil saturation. SPE J. 23 (2), 311–326. https://doi.org/10.2118/10681-PA. Chatzis, I., 2009. Investigation of the mobilization of residual oil using micromodels.

SPE Ann. Tech. Conf. Exhib. https://doi.org/10.2118/129515-STU.
Cheng, Z., Ning, Z., Yu, X., Wang, Q., Zhang, W., 2019. New insights into spontaneous imbibition in tight oil sandstones with N. M.R. J. Petrol. Sci. Eng 179 (1). https://

doi.org/10.1016/j.petrol.2019.04.084.

Du, J., Liu, H., Ma, D., Fu, J., Wang, Y., Zhou, T., 2014. Discussion on effective development techniques for continental tight oil in China. Petrol. Explor. Dev. 41 (2),

198–205. https://doi.org/10.1016/S1876-3804(14)60025-2.

Du, Y., Mehmani, A., Xu, K., Balhoff, M., Torres-Verdin, C., 2019a. Micromodel study of the impacts of fracture connectivity and wettability on matrix sweep effi-

ciency. Unconv. Resour. Technol. Conf. https://doi.org/10.15530/urtec-2019-144.
Du, Y., Xu, K., Mejia, L., Zhu, P., Matthew, T.B., 2019b. Microfluidic investigation of low-salinity effects during oil recovery: a no-clay and time-dependent mechanism. SPE J. 24 (6). https://doi.org/10.2118/197056-PA.

Gao, S., Hu, Z., Guo, W., Zuo, L., Shen, R., 2013. Water absorption characteristics of gas shale and the fracturing fluid flowback capacity. Nat. Gas. Ind. 33 (12), 71–76. https://doi.org/10.3787/j.issn.1000-0976.2013.12.010 (in Chinese).

Garcia, R.B., Andrade, C.T., 1997. Evidence of interaction between agarose and guar

gum from changes in network response to solvent pertubation. Carbohydr. Polym. 34 (3), 157–163. https://doi.org/10.1016/S0144-8617(97)00096-9.

- Grasdalen, H., Painter, T., 1980. NMR Studies of composition and sequence in legume-seed Galactomannans. Carbohydr. Res. 81 (1), 59–66. https://doi.org/10.1016/S0008-6215(00)85677-3.
- He, K., Xu, L., Kenzhekhanov, S., Yin, X., Neeves, K.B., 2017. A rock-on-a-chip approach to study fluid invasion and flowback in liquids-rich shale formations. In: SPE Oklahoma City Oil and Gas Symposium held in Oklahoma City. https://doi.org/10.2118/185088-MS.
- Howe, A.M., Clarke, A., Giernalczyk, D., 2015. Flow of concentrated viscoelastic polymer solutions in porous media: effect of MW and concentration on elastic turbulence onset in various geometries. Soft Matter 11 (32), 6419–6431. https:// doi.org/10.1039/C5SM01042].
- Jia, Y., Song, C., Wang, J., Gan, Q., 2021. The breakdown process of low-permeable shale and high-permeable sandstone rocks due to non-aqueous fracturing: the role of fluid infiltration. J. Nat. Gas Sci. Eng. 89 (4), 103873. https://doi.org/10.1016/i.ingse.2021.103873.
- Kianinejad, A., Ghazanfari, M.H., Kharrat, R., Rashtchian, D., 2013. An experimental investigation of surfactant flooding as a good candidate for enhancing oil recovery from fractured reservoirs using one-quarter five spot micromodels: the role of fracture geometrical properties. Energy Sources 35 (20), 1929—1938. https://doi.org/10.1080/15567036.2010.525591.
- Liang, T., Xu, K., Lu, J., Nguyen, Q., DiCarlo, D., 2019. Evaluating the performance of surfactants in enhancing flowback and permeability after hydraulic fracturing through a microfluidic model. SPE J. 25 (1), 268–287. https://doi.org/10.2118/ 199346-PA.
- Liu, N., Liu, M., Zhang, S., 2015. Flowback patterns of fractured shale gas wells. Nat. Gas. Ind. B 2 (s2–3), 247–251. https://doi.org/10.1016/j.ngib.2015.07.017.
- Longoria, R.A., Liang, T., Nguyen, Q.P., DiCarlo, D.A., 2015. When less flowback is more: a mechanism of permeability damage and its implications on the application of EOR techniques. Unconv. Resour. Technol. Conf. https://doi.org/10.15530/URTEC-2015-2154266.
- Lu, Y., Kang, W., Wu, H., Jiang, J., Zhang, L., 2018. Comprehensive review of acrylamide-based polymer fracturing fluid. Polym. Mater. Sci. Eng. 34 (12), 156–162. https://doi.org/10.16865/j.cnki.1000-7555.2018.12.026.
- Mccleary, B.V., Clark, A.H., Dea, I.C.M., Rees, D.A., 1985. The fine structures of carob and guar galactomannans. Carbohydr. Res. 139, 237–260. https://doi.org/10.1016/0008-6215(85)90024-2
- Mehmani, A., Kelly, S., Torres-Verdin, C., Balhoff, M., 2017. Quantification of fracture-matrix fluid transport in unconventional rocks using two-scale microfluidic chips. Unconv. Resour. Technol. Conf. https://doi.org/10.15530/urtec-2017-2669314
- Morteza, D., 2019. Hydrodynamic dispersion due to a variety of flow velocity profiles in a porous-walled microfluidic channel. Int. J. Heat Mass Tran. 136, 87—98. https://doi.org/10.1016/j.ijheatmasstransfer.2019.02.081.
- Nilsson, M.A., Kulkarni, R., Gerberich, L., Hammond, R., Singh, R., Baumhoff, E., Rothstein, J.P., 2013. Effect of fluid rheology on enhanced oil recovery in a microfluidic sandstone device. J. Non-Newtonian Fluid Mech. 202 (12), 112—119. https://doi.org/10.1016/j.jnnfm.2013.09.011.
- Pak, A., Chan, D.H., 2004. A fully implicit single phase T-H-M fracture model for modelling hydraulic fracturing in oil sands. J. Can. Petrol. Technol. 43 (6), 35–44. https://doi.org/10.2118/04-06-01.
- Schumi, B., Clemens, T., Wegner, J., Ganzer, G., Leitenmüller, V., 2019. Alkali cosolvent polymer flooding of high tan number oil: using phase experiments, micro-models and corefloods for injection agent selection. In: SPE Europec Featured at 81st EAGE Conference and Exhibition. https://doi.org/10.2118/195504-MS.
- Sedaghat, M., Ghazanfari, M., Masihi, M., Rashtchian, D., 2013. Experimental and numerical investigation of polymer flooding in fractured heavy oil five-spot

- systems. J. Petrol. Sci. Eng. 108 (4), 370–382. https://doi.org/10.1016/j.petrol.2013.07.001.
- Sinz, D.K.N., Hanyak, M., Darhuber, A.A., 2013. Self-Induced surfactant transport along discontinuous liquid-liquid interfaces. J. Phys. Chem. Lett. 4 (6), 1039–1043. https://doi.org/10.1021/jz400287x.
- Song, W., Kovscek, A.R., 2015. Functionalization of micromodels with kaolinite for investigation of low salinity oil-recovery processes. Lab Chip 15 (16), 3314–3325. https://doi.org/10.1039/c5lc00544b.
- Tangirala, S., Sheng, J.J., 2019. Investigation of oil production and flowback in hydraulically-fractured water-wet formations using the Lab-on-a-Chip method. Fuel 254. https://doi.org/10.1016/j.fuel.2019.05.126.
- Tompkins, D., Sieker, R., Koseluk, D., Cartaya, H., 2016. Managed pressure flowback in unconventional reservoirs: a Permian Basin case study. Unconv. Resour. Technol. Conf. https://doi.org/10.15530/URTEC-2016-2461207.
- Wang, H., 2015. Numerical modeling of non-planar hydraulic fracture propagation in brittle and ductile rocks using XFEM with cohesive zone method. J. Petrol. Sci. Eng. 135, 127–140. https://doi.org/10.1016/j.petrol.2015.08.010.
  Wang, H., Ma, F., Tong, X., Liu, Z., Zhang, X., Wu, Z., Li, D., Wang, B., Xie, Y., Yang, L.,
- Wang, H., Ma, F., Tong, X., Liu, Z., Zhang, X., Wu, Z., Li, D., Wang, B., Xie, Y., Yang, L., 2016. Assessment of global unconventional oil and gas resources. Petrol. Explor. Dev. 43 (6), 850–862. https://doi.org/10.1016/S1876-3804(16)30111-2.
- Wu, Q., Xu, Y., Wang, X., Wang, T., Zhang, S., 2012. Volume fracturing technology of unconventional reservoirs: connotation, optimization design and implementation, Petrol. Explor. Dev. 39 (3), 352–358 (in Chinese).
- mentation. Petrol. Explor. Dev. 39 (3), 352–358 (in Chinese).

  Xu, G., Jiang, Y., Shi, Y., Han, Y., Wang, M., Zeng, X., 2020. Experimental investigations of fracturing fluid flowback and retention under forced imbibition in fossil hydrogen energy development of tight oil based on nuclear magnetic resonance. Int. J. Hydrogen Energy 45 (24), 13256–13271. https://doi.org/10.1016/i.iihydene.2020.03.054.
- Xu, K., Liang, T., Zhu, P., Qi, P., 2017. A 2.5-D glass micromodel for investigation of multi-phase flow in porous media. Lab Chip 17 (4), 640-646. https://doi.org/ 10.1039/c6lc01476c.
- Zhang, C., Oostrom, M., Wietsma, T.W., Grate, J.W., Warner, M.G., 2011. Influence of viscous and capillary forces on immiscible fluid displacement: pore-scale experimental study in a water-wet micromodel demonstrating viscous and capillary fingering. Acta Ophthalmol. 25 (8), 3493–3505. https://doi.org/ 10.1021/ef101732k.
- Zhang, Y., Ge, H., Shen, Y., Jia, L., 2019. Evaluating the potential for oil recovery by imbibition and time-delay effect in tight reservoirs during shut-in. J. Petrol. Sci. Eng. 184, 106557. https://doi.org/10.1016/j.petrol.2019.106557.
- Zhang, Y., Ge, H., Shen, Y., Mclennan, J., Jia, L., 2020. The retention and flowback of fracturing fluid of branch fractures in tight reservoirs. J. Petrol. Sci. Eng. 198, 108228. https://doi.org/10.1016/j.petrol.2020.108228.
- Zhu, J., Xie, s., Yang, z., Li, X., Chen, J., Zhang, X., Zheng, N., 2021. A review of recent advances and prospects on nanocellulose properties and its applications in oil and gas production. J. Nat. Gas Sci. Eng. 96, 104253. https://doi.org/10.1016/ j.jngse.2021.104253.
- Zou, C., Dong, D., Wang, S., Li, J., Cheng, K., 2010. Geological characteristics, formation mechanism and resource potential of shale gas in China. Petrol. Explor. Dev. 37 (6), 641–653. https://doi.org/10.1016/S1876-3804(12)60001-9.
- Zou, C., Zhang, G., Yang, Z., Tao, S., Wang, Z., 2013. Geological concepts, characteristics, resource potential and key techniques of unconventional hydrocarbon: on unconventional petroleum geology. Petrol. Explor. Dev. 40 (3), 385–399. https://doi.org/10.11698/PED.2013.04.01.
- Zou, C., Yang, Z., Zhu, R., Zhang, G., Hou, L., Wu, S., Tao, S., Yuan, X., Dong, D., Wang, Y., 2015. Progress in China's unconventional oil & gas exploration and development and theoretical technology. Acta Geol. Sin. 89 (6), 979–1007. https://doi.org/10.1111/1755-6724.12491 https://doi.org/CNKI:SUN: DZXE.0.2015-06-001.